2020 American Control Conference
Denver, CO, USA, July 1-3, 2020

Improving fuel economy of heavy-duty vehicles in daily driving

Chaozhe R. He, Anil Alan, Tamás G. Molnár, Sergei S. Avedisov,
A. Harvey Bell, Russell Zukouski, Matthew Hunkler, Jim Yan, and Gábor Orosz

***Abstract*— In this work, we integrate two once separate concepts for longitudinal control of heavy duty vehicles: responding to elevation changes to improve fuel economy using preview and reacting to the motion of preceding vehicles using feedback. The two concepts are unified to provide a safe yet fuel efficient connected and automated technology for heavy duty vehicles. First, we establish an integrated control framework of the two concepts based on barrier function theory and then we discuss the detailed control design of each concept. Finally, we demonstrate the benefits of the proposed design against a naive switching controller by experimentally evaluating the performance of a connected automated truck.**

I. Introduction

It has been shown that by previewing geographical information (i.e., elevation) one can acquire fuel optimal speed profiles for ground vehicles [1–5]. The fuel benefits brought by this approach is particularly beneficial for heavy-duty vehicles. Over the years, many algorithms of different vehicle types and powertrain configurations have been proposed to acquire fuel optimal speed profiles, and many auto manufacturers, including truck makers, have put such preview-based control algorithms into production [6]. These algorithms are often referred to as predictive cruise control (PCC) and use a preview distance of a few kilometers. Typically, 10-15% reduction in fuel consumption can be achieved compared to constant speed cruise control provided no interference from surrounding traffic [3]. However, such fuel benefit may not be attainable in traffic without the driving safety being compromised.

To react to traffic perturbations, connected cruise control (CCC) has been developed that uses motion information from vehicles ahead obtained by sensors as well as wireless vehicle-to-everything (V2X) communication. While the primary goal of CCC is to improve driver comfort and mitigate traffic waves, one may use formal methods to guarantee safety [7–9] and the energy efficiency may also be improved [10]. To specifically target energy consumption, the problem is often formulated as a receding horizon optimal control problem [11,12] utilizing both elevation preview and prediction about preceding vehicle's motion in the next few seconds. While some fuel benefit can be achieved, such an approach relies heavily on the ability to accurately predict the motion of the preceding vehicle [13]. Furthermore, the different spatial/time scales involved when responding to elevation versus traffic limit the benefits: PCC requires minutes of elevation preview while CCC makes decisions at the order of seconds. Such differences can make online optimization very challenging.

In this paper, we make an attempt to integrate the above two concepts, i.e., PCC and CCC, in order to achieve a safe yet fuel efficient connected automated technology. In particular, we adjust the PCC and CCC design structures such that they both present acceleration demands and utilizing barrier function theory [8] we allocate the two functionalities in real time. The remainder of this paper is organized as follows. After briefly introducing the vehicle dynamics and fuel consumption models in Section II, we describe the PCC and CCC designs and their integration in Section III. Then we describe the experimental setup in Section IV and present the experimental results in Section V. We conclude the study and discuss future work in Section VI.

II. Modeling

In this section, we describe the mathematical models used in this paper, including vehicle dynamics, fuel consumption maps and input/state constraints.

The longitudinal dynamics of the truck are derived using classical mechanics. We assume that no slip occurs at the wheels and that the flexibility of the tires and the suspension can be neglected. Then using the power law we obtain

$$m_{\rm eff}\dot{v} = -mg\sin\phi - \gamma mg\cos\phi - k_0(v+v_{\rm w})^2 + \frac{\eta T_{\rm e} + T_{\rm b}}{R}, \quad (1)$$

see [3], where the dot denotes differentiation with respect to time t. The effective mass $m_{\rm eff} = m + I/R^2$ contains the mass of the vehicle m, the moment of inertia I of the rotating elements, and the wheel radius R. Furthermore, g is the gravitational constant, ϕ is the inclination angle, γ is the rolling resistance coefficient, k_0 is the air drag constant, $v_{\rm w}$ is the speed of the headwind, η is the gear ratio (that includes the final drive ratio and the transmission efficiency). The engine torque $T_{\rm e}$ is assumed to be non-negative while the braking torque $T_{\rm b}$ applied on the axle is assumed to be non-positive. Based on (1), we have

$$\dot{v} = -a\sin\phi - b\cos\phi - k\,(v+v_{\rm w})^2 + \hat{u}, \quad (2)$$

where

$$a = \frac{mg}{m_{\rm eff}}, \quad b = \frac{\gamma\, mg}{m_{\rm eff}}, \quad k = \frac{k_0}{m_{\rm eff}}, \quad \hat{u} = \frac{\eta T_{\rm e} + T_{\rm b}}{m_{\rm eff} R}. \quad (3)$$

This work was supported by the Navistar, Inc.

Chaozhe He, Anil Alan, Tamás Molnár, Sergei Avedisov, Harvey Bell, and Gábor Orosz are with the Department of Mechanical Engineering, University of Michigan, Ann Arbor, MI 48109 {hchaozhe, anilalan, molnart, avediska, ahbelliv, orosz} @umich.edu

Matthew Hunkler, Russell Zukouski, and Jim Yan are with Navistar, Inc. Lisle, 60532 {Matthew.Hunkler, Russ.Zukouski, Jim.Yan} @Navistar.com

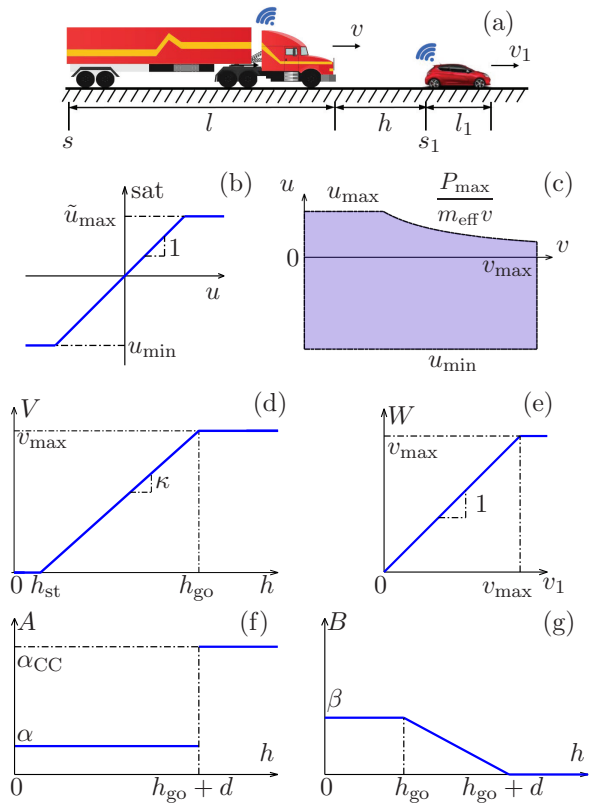

Fig. 1: (a) A truck driving behind a human-driven vehicle on a single-lane road. (b,c) The saturation functions (6,7). (d) The range policy function (19). (e) The saturation function (20). (f,g) The feedback gains (21) and (22).

According to the specifications of a ProStar truck manufactured by Navistar (see [3]) we use the parameter values $a = 9.6416[\mathrm{m/s^2}]$, $b = 0.0578[\mathrm{m/s^2}]$, $k = 4.1987 \times 10^{-4}[1/\mathrm{m}]$ and we assume no headwind, i.e., $v_\mathrm{w} = 0$.

Since the inclination angle ϕ is a function of the distance travelled s, the equation of motion becomes

$$\begin{aligned} \dot{s} &= v, \\ \dot{v} &= -f(s,v) + \mathrm{sat}(u), \end{aligned} \tag{4}$$

where s denotes the position of the rear bumper of the truck (see Fig. 1(a)) and

$$f(s,v) = a \sin\phi(s) + b\cos\phi(s) + kv^2. \tag{5}$$

Moreover, u denotes the control input which saturates due to the torque and power limits of the engine and the torque limits of the brakes, that is,

$$\mathrm{sat}(u) = \begin{cases} u_{\min} & \text{if} \quad u \le u_{\min}, \\ u & \text{if} \quad u_{\min} < u < \tilde{u}_{\max}, \\ \tilde{u}_{\max} & \text{if} \quad u \ge \tilde{u}_{\max}, \end{cases} \tag{6}$$

where

$$\tilde{u}_{\max} = \min\left\{u_{\max}, \frac{P_{\max}}{m_{\mathrm{eff}} v}\right\}, \tag{7}$$

see Fig. 1(b,c). In this work, we enforce $u_{\max} = 2[\mathrm{m/s^2}]$ and $u_{\min} = -3[\mathrm{m/s^2}]$ and we have $P_{\max}/m_{\mathrm{eff}} = 0.010143$ [kW/kg]. Finally, the speed limit $v_{\max}$ is enforced according to the position s along the road, that is, we require

$$0 \le v(s) \le v_{\max}(s). \tag{8}$$

Fuel consumption rates are typically given as a function of the engine speed ω_e and engine torque T_e, that is, $q(\omega_\mathrm{e}, T_\mathrm{e})$. Given a well defined gear shift logic one may obtain the fuel consumption as a function of the speed v and the control input u, i.e., $q(v,u)$; see [14]. Here we utilize the Willans approximation (see [15]):

$$q(v,u) = p_2 v\, g(u) + p_1 v, \tag{9}$$

where the nonsmooth function $g(x) = \max(0,x)$ represents that for $u < 0$ the engine torque is set to zero and the brakes are applied. To bypass this nonsmoothness in the optimization, we define the control inputs u_d and u_b such that

$$u = u_\mathrm{d} + u_\mathrm{b}, \tag{10}$$

with the constraints

$$u_\mathrm{d} \ge 0, \quad u_\mathrm{b} \le 0, \quad u_\mathrm{d} u_\mathrm{b} = 0. \tag{11}$$

Indeed, u_d is related to engine torque while u_b is related to braking torque; cf. (2,3). For our truck we have p_2=1.8284 [$\mathrm{gs^2/m^2}$], p_1=0.0209 [g/m].

III. Integrated Control Design

In this section, we first introduce our strategy to integrate controllers of different objectives. Then we describe the details of the predictive cruise control (PCC) that is based on elevation preview as well as the connected cruise control (CCC) that responds to the motion of preceding vehicles.

Considering the vehicle dynamics (4) one may design a controller of the form

$$u(t) = \tilde{f}\big(s(t-\zeta), v(t-\zeta)\big) + a_\mathrm{d}(t-\zeta), \tag{12}$$

where ζ lumps the communication delay and the actuator delay; see [16,17]. The term $\tilde{f}(s,v)$ is designed to compensate for the resistance term $f(s,v)$ while a_d denotes the higher-level acceleration demand. Due to their different objectives (e.g., fuel economy vs. safety) higher level controllers may demand different acceleration values.

Assume that there are n different control designs available with different objectives and they each provide an acceleration demand $a_{i,\mathrm{d}}$. Then we consider the integrated controller

$$a_\mathrm{d} = \min_{i=1,\cdots,n} \{a_{i,\mathrm{d}}\}. \tag{13}$$

Notice that this controller is independent of the individual control designs, each of which makes its own decision according to its own objective. This strategy is an extension to the min-norm controller based on quadratic program (QP) established in [8,18] and to the minimum intervention control presented in [9]. In the min-norm controller, safety is ensured by introducing the control barrier function condition as a constraint to QP formulation. The optimization problem can

be formulated in a way that the solution is optimal in the sense of how far it deviates from a given nominal controller. In this scenario, PCC is considered to be the nominal control, whereas CCC is utilized to be the resulting control solution when the barrier constraint is active, which means safety – as defined by the barrier function – is no longer achievable with PCC. The strategy is practical not only due to its simplicity, but also because it can integrate designs that are inherently different.

Specifically, assuming that both the CCC and PCC designs provide acceleration demands, namely a_{CCC} and a_{PCC}, we propose the controller

$$a_{\mathrm{d}} = \min\left\{a_{\mathrm{CCC}}, a_{\mathrm{PCC}}\right\}. \tag{14}$$

This handles the time scale difference between the CCC design (few seconds and few hundred meters) versus the PCC design (few minutes and few kilometers). While one may design different switching logics based on the states used in the individual controllers, we demonstrate below that our integration can outperform such strategies without requiring extensive tuning.

A. Predictive Cruise Control Algorithm

The predictive cruise control design is formulated as an optimal control framework, that gives the fuel optimal speed profile over a preview distance while taking into account elevation. To reduce computational complexity, we convert time based models to distance based ones. Combining the models introduced in Section II, we formulate the following optimal control problem:

$$\begin{aligned}
\min_{u_{\mathrm{d}}, u_{\mathrm{b}}} \; & J = \int_0^{s_{\mathrm{f}}} \frac{q(v, u_{\mathrm{d}})}{v}\,\mathrm{d}s, \\
\text{subject to} \quad & \frac{\mathrm{d}v}{\mathrm{d}s} = \frac{-f(s,v) + u_{\mathrm{d}} + u_{\mathrm{b}}}{v}, \\
& \int_0^{s_{\mathrm{f}}} \frac{1}{v}\,\mathrm{d}s \le t_{\mathrm{f}}, \\
& u_{\min} \le u_{\mathrm{b}} \le 0, \\
& 0 \le u_{\mathrm{d}} \le \min\left\{u_{\max}, \frac{P_{\max}}{m_{\mathrm{eff}} v}\right\}, \\
& v_{\min} \le v(s) \le v_{\max}(s), \\
& v(0) = v_0, \\
& v(t_{\mathrm{f}}) = v_{\mathrm{f}}.
\end{aligned} \tag{15}$$

Here, s_{f} is the preview distance, $v_{\min} > 0$ is the lower speed limit, v_0 and v_{f} are vehicle speeds at the time when the optimal control problem is formulated and at the end of preview distance, respectively. To ensure that travel time is not sacrificed for better fuel economy, we prescribe the upper bound t_{f} for total travel time as a constraint. For example, one may set the upper bound $t_{\mathrm{f}} = s_{\mathrm{f}}/v_{\mathrm{CC}} + \Delta t$ where v_{CC} is a pre-defined cruise control set speed and Δt is a slack variable. Previous studies have shown that such setup is effective in providing fuel efficient speed trajectories [3]. We remark that when substituting the approximation (9) into the cost function in (15) the second term becomes a constant. Thus, after dropping the constant p_1, one may redefine the cost function as $\int_0^{s_{\mathrm{f}}} u_{\mathrm{d}}\,\mathrm{d}s$.

In order to solve the above optimal control problem we discretize space with $\Delta s \approx 2.5[\mathrm{m}]$ and the resulting nonlinear programming problem is solved by the open-source interior point solver IPOPT [19]. Apart from the control input u_{d} and u_{b}, we also obtain the optimal speed profile v_{PCC} as function of the distance s. For real-time implementation, this speed profile is followed using a cruise controller with gain α_{CC}:

$$a_{\mathrm{PCC}} = \alpha_{\mathrm{CC}}(v_{\mathrm{PCC}}(s) - v). \tag{16}$$

B. Connected Cruise Control Algorithm

The connected cruise controller is given in [10] when a connected automated vehicle is responding to multiple vehicles ahead. For the sake of simplicity here we consider the case when the truck only responds to the vehicle immediately ahead using the feedback law

$$a_{\mathrm{CCC}} = A\big(V(h) - v\big) + B\big(W(v_1) - v\big). \tag{17}$$

Here, h denotes the distance headway, that is, the bumper-to-bumper distance between the truck and the preceding vehicle:

$$h = s_1 - s - l. \tag{18}$$

Here l is the length of the truck and s_1 denotes the position of the rear bumper of the preceding vehicle; see Fig. 1(a).

The range policy function

$$V(h) = \begin{cases} 0 & \text{if} \quad h \le h_{\mathrm{st}}, \\ \kappa(h - h_{\mathrm{st}}) & \text{if} \quad h_{\mathrm{st}} < h < h_{\mathrm{go}}, \\ v_{\max} & \text{if} \quad h \ge h_{\mathrm{go}}, \end{cases} \tag{19}$$

describes the desired velocity of the truck as a function of its headway; see Fig. 1(d). For a small headway ($h < h_{\mathrm{st}}$), the truck intends to stop; for a large headway ($h > h_{\mathrm{go}}$), it intends to travel with the speed limit $v_{\max}$; between h_{st} and h_{go} the desired velocity increases linearly, with the gradient κ. As mentioned above $v_{\max}$ varies according to position s (cf. (8)) which yields $h_{\mathrm{go}}(s) = h_{\mathrm{st}} + v_{\max}(s)/\kappa$. The saturation function

$$W(v_1) = \begin{cases} v_1 & \text{if} \quad v_1 \le v_{\max}, \\ v_{\max} & \text{if} \quad v_1 > v_{\max}, \end{cases} \tag{20}$$

shown in Fig. 1(e) is included to enforce the speed limit even when a preceding vehicle is speeding.

The feedback gains A and B in (17) are designed to vary with distance in order to make a smooth transition between CCC and cruise control:

$$A(h) = \begin{cases} \alpha & \text{if} \quad h \le h_{\mathrm{go}} + d, \\ \alpha_{\mathrm{CC}} & \text{if} \quad h > h_{\mathrm{go}} + d, \end{cases} \tag{21}$$

$$B(h) = \begin{cases} \beta & \text{if} \quad h \le h_{\mathrm{go}}, \\ \beta\dfrac{h_{\mathrm{go}} + d - h}{d} & \text{if} \quad h_{\mathrm{go}} < h < h_{\mathrm{go}} + d, \\ 0 & \text{if} \quad h \ge h_{\mathrm{go}} + d; \end{cases} \tag{22}$$

see Fig. 1(f,g). We summarize the numerical values of the parameters used in (19,20,21,22) in Table I. We remark that

α	0.4 [1/s]	κ	0.6 [1/s]
β	0.5 [1/s]	d	20 [m]
$u_{\max}$	2 [m/s^2]	$u_{\min}$	-3 [m/s^2]
h_{st}	5[m]	$v_{\min}$	2.24 [m/s] = 5 [mph]

TABLE I: Parameters used in this paper.

while κ and α were set considering driver comfort and safety, parameter β was optimized to maintain good fuel economy while responding to the motion of the preceding vehicle [13].

IV. Experimental Setup

In this section, we describe the experimental setup used to test the above controller design. We first discuss the hardware structure of the connected automated truck. We then briefly introduce the lower level acceleration tracking control design. After describing the test environment and maneuvers, we present the evaluation method for energy efficiency.

The test truck was developed from a 2011 ProStar+ in-production truck, whose powertrain corresponds to the parameters used in the Section II; see Fig. 2. A Navistar PCC box with internal database of main road geometry provides elevation previews, as well as hosts the PCC algorithm. Vehicle-to-vehicle (V2V) connectivity is used to detect the preceding vehicle and measure the distance h and the velocities v, v_1. A Speedgoat real time machine is used to run the core algorithm as well as the lower-level controller using MATLAB Simulink RealTime Toolbox. It receives V2V data through user datagram protocol (UDP) while it transmits PCC results using J1939 CAN protocol.

The engine and brake control are enabled such that they take desired engine torque $T_{\text{e,d}}$ and brake pressure p_{brake} as inputs through the J1939 CAN protocol. The acceleration demand a_{d} given by the integrated PCC and CCC design (14) is given to a lower level controller that compensates for the elevation using (5,12). Then with two feedforward maps acquired from calibration, the desired engine torque $T_{\text{e,d}} = f_{\text{prop}}(u, v)$ and brake pressure $p_{\text{brake}} = f_{\text{brake}}(u, v)$ are calculated; see the "Algorithm" block in Fig. 2.

To conduct the experiments, we selected a route at Navistar Proving Grounds, which has significant elevation changes as shown in Fig. 3(a,b). Due to the road surface variations and turns along the route (see Fig. 3(a)), we enforce a customized speed limit shown by the black curve in Fig. 3(c). This speed limit is incorporated into both the PCC and the CCC design. Considering the elevation profile and the speed limits, the PCC algorithm (15) provides the planned speed profile shown by the dashed gray curve in Fig. 3(c).

To trigger the CCC functionality, a preceding vehicle is driven along the route as shown by the purple curve in Fig. 3(c). This speed profile is based on the behavior of the preceding vehicle's driver when obeying the traffic signs and the speed limit. The symbols in Fig. 3 highlight events in the motion of the preceding vehicle: start/finish (green triangles), slowdowns (purple triangles), turns (blue triangles), and complete stops (red squares). The experimental setup allows us to record the preceding vehicle's speed profile and replay the data from the record. This way we can keep consistency

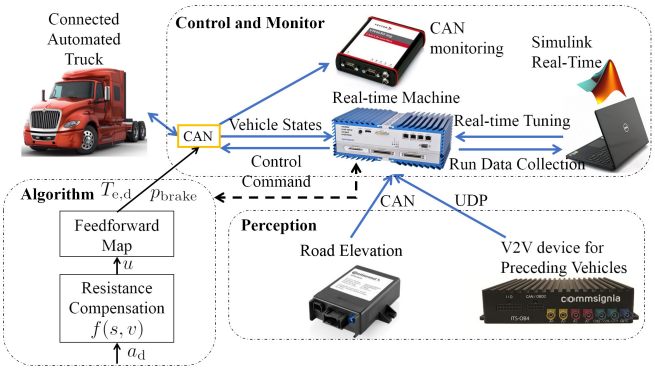

Fig. 2: Architecture of the connected automated truck.

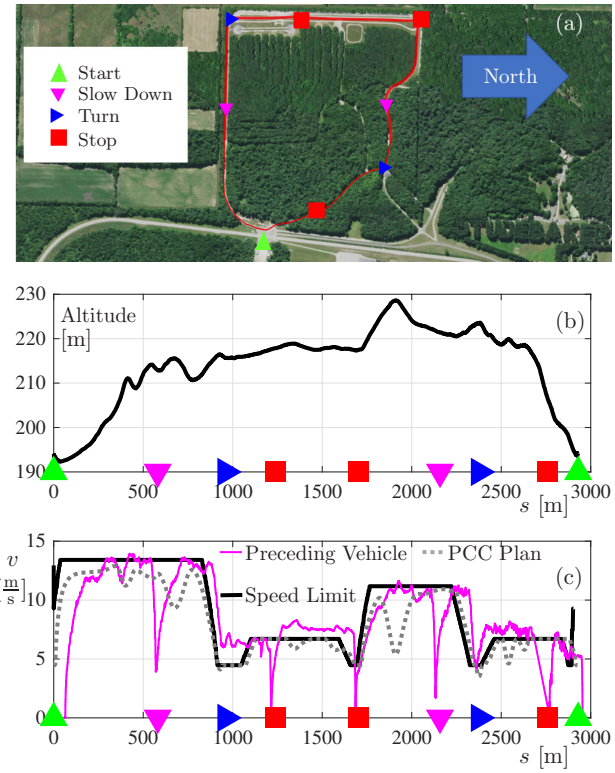

Fig. 3: (a) The test route at the Navistar Proving Grounds. (b) The corresponding elevation profile. (c) The speed profile of the preceding vehicle, the speed limit, and the planned PCC profile as a function of the distance traveled. Green triangles – start/finish, purple triangles – slowdowns, blue triangles – turns, red squares – stops.

amongst subsequent experiments and compare the energy savings of different control designs. This unique feature resulted from our V2V based test platform setup. To assess the effects of variations in the preceding vehicle's motion we also ran the experiments with the driver trying to repeat the same speed profile.

For simplicity, we run the PCC algorithm (15) offline to generate the optimal speed profile for the entire route rather than using the real-time optimization. This way we ensure that the improvement of energy efficiency is due to the PCC and CCC integration, rather than the PCC and

CCC algorithms themselves. The parameter $t_\mathrm{f} = 400[\mathrm{s}]$ is determined based on the travel time of the preceding vehicle.

In order to evaluate the energy efficiency, we define the cumulative energy consumption per unit mass for the truck in time scale as

$$w(t) = \int_0^t u_\mathrm{d} v \,\mathrm{d}\tilde{t} = \int_0^t g(u) v \,\mathrm{d}\tilde{t} = \int_0^t g\big(\dot{v} + f(s,v)\big) v \,\mathrm{d}\tilde{t}. \tag{23}$$

With the conversion to spatial scale using $w(t) = w(s(t))$, where $s(t) = \int_0^t v \,\mathrm{d}\tilde{t}$, (23) corresponds to the cost function in (15) with the Willans approximation (9). In the last step we used model (4) to calculate the energy consumption based on the kinematic quantities. The effectiveness of this approach for designing fuel efficient control algorithms was demonstrated in previous studies [10,13].

V. Experimental Results

In this section, we present the experimental results. We ran two sets of experiments: in the first case a virtual preceding vehicle is considered, while in the second case a real human-driven vehicle is utilized. In both cases we ran four different types of experiments: "PCC" tries to follow the velocity profile $v_\mathrm{PCC}(s)$ generated by (15) using (16); "CCC" uses algorithm (17); the "Integrated Design" utilizes (14); while the "Naive Switch" refers to a simple time headway-based switch between PCC and CCC as explained further below.

Figure 4 shows experimental results for a PCC run (green) and a CCC run (red), along with a run using the proposed integrated design (blue). Panel (a) shows the realized speed profiles, while panel (b) shows the corresponding energy consumption. Without the presence of a preceding vehicle, the truck closely follows the planned PCC profile; cf. green curve on Fig. 4 and the gray dashed curve in Fig. 3(c). Indeed, the PCC run (green) has the lowest energy consumption among the runs shown in Fig. 4(b). One may notice though that the executed PCC run consumes more energy compared to the planned profile which we attribute to the fidelity of the simple model (4) (no gear changes, no engine dynamics) used in the optimization (15) and the time delays in (12,16).

The CCC run (red) performs the worst in terms of energy consumption as in this case the truck keeps responding to the motion of the preceding vehicle that is particularly obvious at the slow downs (purple triangles) and the stops (red squares); cf. red curve in Fig. 4 and the purple curve in Fig. 3(c). The energy consumption of the integrated design (blue) is close to that of the PCC (green) as the truck manages to stay in PCC mode most of the time and only responds to the preceding vehicle when necessary. This is particularly visible at the slow downs and the stops where the integrated design requires less braking and acceleration compared to the CCC, resulting in the corresponding energy curves to deviate from each other.

The experiments with PCC, CCC, and integrated design were repeated multiple times to evaluate the uncertainty of the experimental results and for each run the total energy consumption was calculated. Table II shows the mean value and the standard deviation of the total energy consumption as

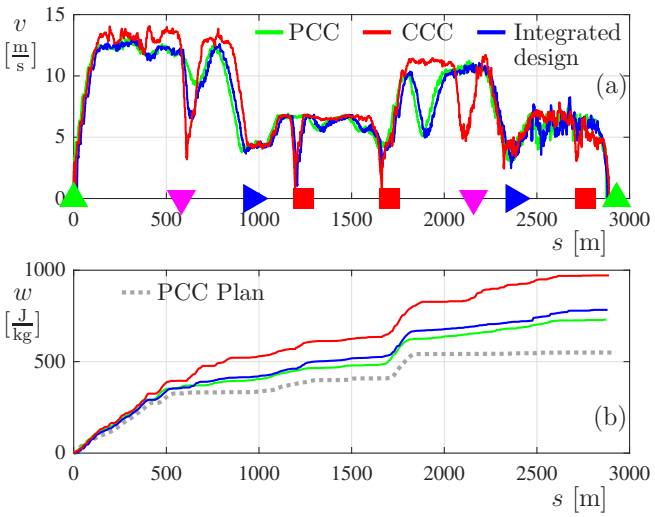

Fig. 4: (a) Speed profiles for PCC (green), CCC (red), and an integrated design (blue) for a virtual preceding vehicle. (b) The corresponding energy consumption curves as a function of distance traveled. The gray dashed curve corresponds to the planned PCC profile depicted in Fig. 3(c).

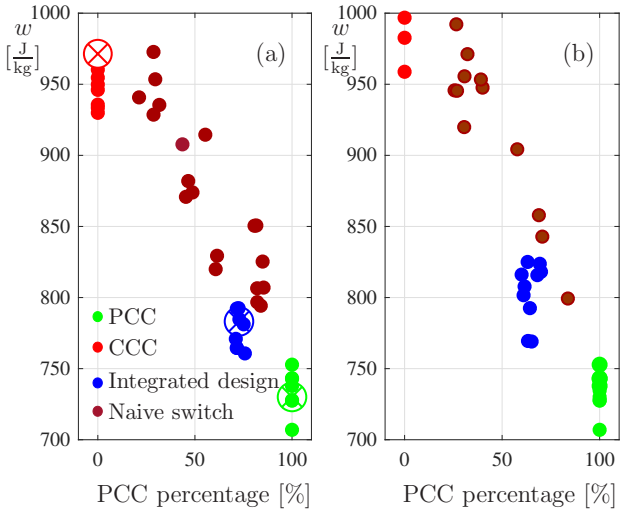

Fig. 5: Total energy consumption as a function of PCC percentage for different experiments. (a) Responding to a virtual preceding vehicle. (b) Responding to a human-driven vehicle. The crosses correspond to Fig. 4(b).

well as the energy savings compared to CCC. The proposed integrated design provides approximately 18% benefit in energy consumption, which is consistently observed over multiple experiments. To further analyze the impact of the integrated design, the percentage of the total PCC time over the whole run is also calculated. Figure 5(a) summarizes these results by plotting the total energy consumption against the PCC percentage for all runs so that crosses correspond to the final values in Fig. 3(b). The integrated design achieves its benefits while spending approximately 75% of the time in PCC.

The same set of experiments were also carried out with a human-driven preceding vehicle trying to replicate the

Preceding car	Controller	Mean $[\frac{\text{J}}{\text{kg}}]$	Standard deviation $[\frac{\text{J}}{\text{kg}}]$	Energy saving [%]
Virtual	CCC	948	14	
	Integrated design	779	12	18 ± 3
	PCC	734	13	23 ± 4
				25 ± 4
Human	CCC	979	19	
	Integrated design	804	21	18 ± 5

TABLE II: Energy consumption of the different designs.

speed profile in Fig. 3(c). This demonstrates the effects of uncertainties in the preceding vehicle's motion. The total energy consumption values as a function of PCC percentage are depicted in Fig. 5(b). Similar conclusions can be drawn for these experiments as above: the PCC and CCC tests form boundaries in terms of energy consumption, and the proposed integrated design gives energy consumption values close to the PCC runs. While having a human driver in the preceding car results in more scatter in the energy consumption, the results are quite similar to those obtained for virtual driver, demonstrating the robustness of the proposed integrated design. This is also reflected by the numbers listed in Table II where again 18% of energy saving is observed on average.

A. Comparison to "Naive Switch"

Finally, we compare our integrated design to another design which implements a naive switch between PCC and CCC based on the speed v and the distance headway h. In particular we implement the time headway-based switch

$$a_{\text{d}} = \begin{cases} a_{\text{CCC}} & \text{if} \quad h \leq v/\overline{\kappa}_{\text{sw}} + \overline{h}_{\text{sw}}, \\ a_{\text{PCC}} & \text{if} \quad h > v/\overline{\kappa}_{\text{sw}} + \overline{h}_{\text{sw}}. \end{cases} \tag{24}$$

Note that in this design the PCC and CCC functionalities are not integrated but simply turned on and off using (24).

Experiments with the naive switch are conducted by choosing $\overline{h}_{\text{sw}} = 10$ [m] and multiple different $\overline{\kappa}_{\text{sw}}$ values within the interval $[1/10,\ 3/5]$ [1/s]. Results are shown by brown color in Fig. 5(a) and (b) for virtual and for the human-driven preceding vehicles, respectively. One may observe that increasing $\overline{\kappa}_{\text{sw}}$ increases the PCC percentage and decreases the overall energy consumption, but the energy benefits are increasing at the expense of reducing driver comfort. Still, since not only the percentage of PCC is important but the part of the road where it is used, the integrated design outperforms the benchmark design in terms of energy consumption without compromising comfort.

VI. Conclusion

In this paper, we proposed a simple yet effective integration of predictive cruise control and connected cruise control to enable fuel efficient operation while maintaining safety in traffic. Experimental results showed robust improvement in energy efficiency by the proposed method when compared to a time headway-based switch. In the future, we would like to extend the design to fully loaded tractor-trailer configuration and test in real traffic scenarios over more complex elevation profiles.

Acknowledgement

The authors would like to thank Commsignia, Inc., and Mechanical Simulation for their technical support. Chaozhe He would like to acknowledge the valuable discussions with Brendan Chan, Daniel Kang, Eric Jiang at Navistar, Inc.

References

[1] E. Hellström, "Look-ahead control of heavy vehicles," Ph.D. dissertation, Linköping University, Sweden, 2010.

[2] A. Sciarretta, G. De Nunzio, and L. Ojeda, "Optimal ecodriving control: Energy-efficient driving of road vehicles as an optimal control problem," *IEEE Control Systems Magazine*, vol. 35, no. 5, pp. 71–90, 2015.

[3] C. R. He, H. Maurer, and G. Orosz, "Fuel consumption optimization of heavy-duty vehicles with grade, wind, and traffic information," *Journal of Computational and Nonlinear Dynamics*, vol. 11, no. 6, p. 061011, 2016.

[4] A. Sciarretta and A. Vahidi, *Energy-Efficient Driving of Road Vehicles*. Springer, 2020.

[5] A. Vahidi and A. Sciarretta, "Energy saving potentials of connected and automated vehicles," *Transportation Research Part C*, vol. 95, pp. 822–843, 2018.

[6] U.S. Department of Energy, "Vehicle technologies office: Fact sheet on adoption of new fuel-efficient technologies from supertruck," June 2016.

[7] P. Nilsson, O. Hussien, A. Balkan, Y. Chen, A. D. Ames, J. W. Grizzle, N. Ozay, H. Peng, and P. Tabuada, "Correct-by-construction adaptive cruise control: Two approaches," *IEEE Transactions on Control Systems Technology*, vol. 24, no. 4, pp. 1294–1307, 2016.

[8] A. D. Ames, X. Xu, J. W. Grizzle, and P. Tabuada, "Control barrier function based quadratic programs for safety critical systems," *IEEE Transactions on Automatic Control*, vol. 62, no. 8, pp. 3861–3876, 2017.

[9] C. R. He and G. Orosz, "Safety guaranteed connected cruise control," in *Proceedings of the International Conference on Intelligent Transportation Systems*, 2018, pp. 549–554.

[10] J. I. Ge, S. S. Avedisov, C. R. He, W. B. Qin, M. Sadeghpour, and G. Orosz, "Experimental validation of connected automated vehicle design among human-driven vehicles," *Transportation Research Part C*, vol. 91, pp. 335–352, 2018.

[11] S. E. Li, Z. Jia, K. Li, and B. Cheng, "Fast online computation of a model predictive controller and its application to fuel economy-oriented adaptive cruise control," *IEEE Transactions on Intelligent Transportation Systems*, vol. 16, no. 3, pp. 1199–1209, 2015.

[12] J. Jing, E. Özatay, A. Kurt, J. Michelini, P. F. Dimitre, and Ü. Özgüner, "Design of a fuel economy oriented vehicle longitudinal speed controller with optimal gear sequence," in *Proceedings of the IEEE Conference on Decision and Control*, 2016, pp. 1595–1601.

[13] C. R. He, J. I. Ge, and G. Orosz, "Fuel efficient connected cruise control for heavy-duty trucks in real traffic," *IEEE Transactions on Control Systems Technology*, pp. 1–8, 2019.

[14] C. R. He, W. B. Qin, N. Ozay, and G. Orosz, "Optimal gear shift schedule design for automated vehicles: Hybrid system based analytical approach," *IEEE Transactions on Control Systems Technology*, vol. 26, pp. 2078–2090, 2018.

[15] L. Guzzella and C. H. Onder, *Introduction to Modelling and Control of Internal Combustion Engine Systems*. Springer, 2004.

[16] G. Orosz, "Connected cruise control: modelling, delay effects, and nonlinear behaviour," *Vehicle System Dynamics*, vol. 54, no. 8, pp. 1147–1176, 2016.

[17] S. E. Li, Q. Guo, S. Xu, J. Duan, S. Li, C. Li, and K. Su, "Performance enhanced predictive control for adaptive cruise control system considering road elevation information," *IEEE Transactions on Intelligent Vehicles*, vol. 2, no. 3, pp. 150–160, 2017.

[18] A. D. Ames, S. Coogan, M. Egerstedt, G. Notomista, K. Sreenath, and P. Tabuada, "Control barrier functions: Theory and applications," in *Proceedings of the European Control Conference*, 2019, pp. 3420–3431.

[19] A. Wächter and L. T. Biegler, "On the implementation of an interior-point filter line-search algorithm for large-scale nonlinear programming," *Mathematical Programming*, vol. 106, no. 1, pp. 25–57, 2006.